Measurement of High-Pressure Shock Waves in Cryogenic Deuterium-Tritium Ice Layered Capsule Implosions on NIF

H. F. Robey,[1,*] J. D. Moody,[1] P. M. Celliers,[1] J. S. Ross,[1] J. Ralph,[1] S. Le Pape,[1] L. Berzak Hopkins,[1] T. Parham,[1] J. Sater,[1] E. R Mapoles,[1] D. M. Holunga,[1] C. F. Walters,[1] B. J. Haid,[1] B. J. Kozioziemski,[1] R. J. Dylla-Spears,[1] K. G. Krauter,[1] G. Frieders,[1] G. Ross,[1] M. W. Bowers,[1] D. J. Strozzi,[1] B. E. Yoxall,[1] A. V. Hamza,[1] B. Dzenitis,[1] S. D. Bhandarkar,[1] B. Young,[1] B. M. Van Wonterghem,[1] L. J. Atherton,[1] O. L. Landen,[1] M. J. Edwards,[1] and T. R. Boehly[2]

[1]*Lawrence Livermore National Laboratory, Livermore, California 94551, USA*
[2]*Laboratory for Laser Energetics, Rochester, New York 14623, USA*

(Received 22 March 2013; published 7 August 2013)

The first measurements of multiple, high-pressure shock waves in cryogenic deuterium-tritium (DT) ice layered capsule implosions on the National Ignition Facility have been performed. The strength and relative timing of these shocks must be adjusted to very high precision in order to keep the DT fuel entropy low and compressibility high. All previous measurements of shock timing in inertial confinement fusion implosions [T. R. Boehly *et al.*, Phys. Rev. Lett. **106**, 195005 (2011), H. F. Robey *et al.*, Phys. Rev. Lett. **108**, 215004 (2012)] have been performed in surrogate targets, where the solid DT ice shell and central DT gas regions were replaced with a continuous liquid deuterium (D2) fill. This report presents the first experimental validation of the assumptions underlying this surrogate technique.

DOI: 10.1103/PhysRevLett.111.065003 PACS numbers: 52.57.−z, 06.30.Gv, 52.35.Tc

Capsule implosions on the National Ignition Facility (NIF) are underway using the indirect-drive concept [1], where the energy of a temporally shaped laser pulse from 192 NIF beams is converted into thermal x rays in a cylindrical high-Z (Au or U) enclosure (hohlraum), as illustrated in the inset of Fig. 1(a). The hohlraum dimensions for recent NIF implosions are 9.4 mm in length by 5.75 mm in diameter with the laser beams entering the hohlraum through two laser entrance holes of diameter 3.1 mm. The x-ray radiation uniformly ablates the surface of a low-Z (CH) spherical ablator shell ($r = 1.1$ mm), which surrounds a spherical cryogenic layer of solid DT fuel (70 μm thickness, $T = 18.7$ K, $\rho = 0.255$ g/cm^3) and central low-density (0.3 mg/cm^3) DT gas fill. The hohlraum x-ray drive spherically compresses the fuel to create the high density and temperature plasma conditions required to initiate DT fusion reactions in the hot, compressed central fuel core. The laser drive consists of four pulses of increasing energy as shown in the inset of Fig. 1(a). These pulses drive a sequence of four shock waves into the ablator and DT fuel to compress it while maintaining low entropy and a low adiabat (ratio of fuel pressure to the Fermi degenerate pressure). Figure 1(a) shows the desired shock trajectories (plotted relative to the $t = 0$ material boundaries: CH ablator, DT ice, DT gas) from a 1D numerical simulation using the radiation-hydrodynamics code HYDRA [2]. The shocks and rarefactions are visualized by plotting the absolute value of the radial pressure gradient, $|\frac{1}{P}\frac{dP}{dr}|$. The four shocks are tuned to traverse the DT ice layer sequentially, coalescing just after transit of the layer. Mistiming of the shocks results in increased fuel entropy and reduced compressibility, which severely degrades the prospects for ignition.

To experimentally diagnose and adjust the strength and timing of these shocks, a modified hohlraum geometry is used as shown in the inset of Fig. 1(b). A Au diagnostic cone is added, penetrating both the hohlraum and capsule walls, to allow for the direct measurement of shock propagation in the capsule interior. Following the technique first described in [3], the capsule and Au cone are filled with liquid deuterium (D2) at $T = 21.5$ K and $\rho = 0.170$ g/cm^3 (replacing the DT ice and gas of an ignition capsule), and the VISAR (Velocity Interferometer System for Any Reflector) diagnostic [4,5] is used to optically measure the velocity vs time of the highly reflective leading shock front [6]. The shape of the D2-filled region is similar to that of an old-fashioned "keyhole"; hence this target has become known as the keyhole hohlraum. Initial experiments demonstrating the shock measurement technique and its application to shock tuning for directly driven implosions on the OMEGA Laser Facility are reported in [7,8]. Details of the modifications required for the higher power environment encountered in indirectly driven implosions on NIF and initial tuning results for NIF ignition pulses are given in [9,10].

Figure 1(b) shows the corresponding simulated shock trajectories in the keyhole target for the same laser drive as shown in Fig. 1(a). Predicted shock trajectories are very similar, though not identical, in the ignition and surrogate tuning geometries, with the obvious exception of the rarefaction fan that results as the first shock transits the strong density discontinuity at the DT ice-gas interface of an ignition target. This rarefaction is completely absent in the continuous D2 fill of the tuning target. The inset list in Fig. 1(b) compares the predicted velocities (μm/ns) of each shock between the D2 and DT-filled targets. The

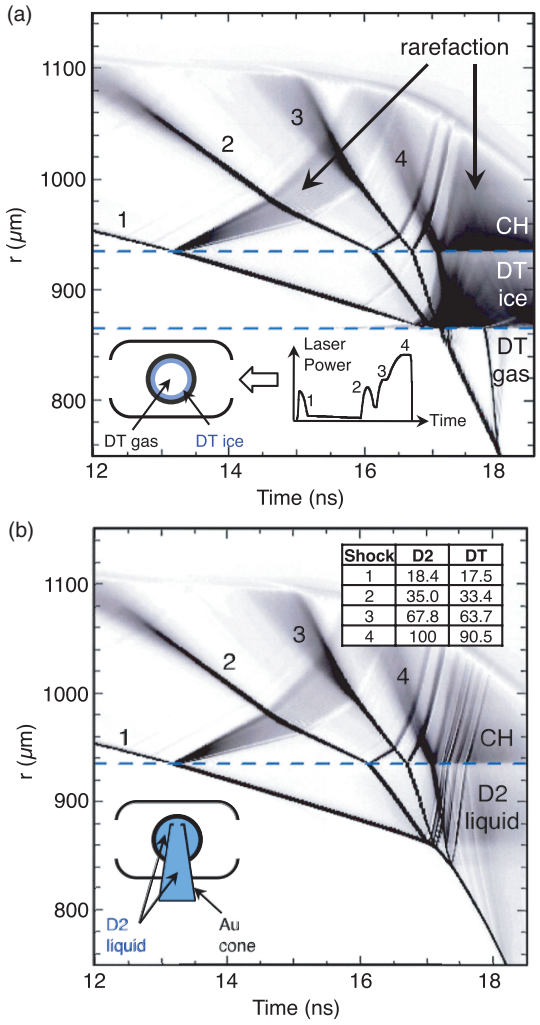

FIG. 1 (color). (a) Simulated shock trajectories in a DT layered ignition capsule. Inset shows the geometry of a NIF ignition hohlraum and the laser pulse. (b) Simulated shock trajectories in the keyhole tuning hohlraum. Inset shows Au diagnostic cone and ablator, both filled with liquid deuterium. Inset list compares velocities (μm/ns) of the 4 shocks between liquid D2 and DT ice.

velocities measured in the less dense D2 liquid are slightly higher than in the more dense DT ice, as expected from the solution of the Riemann problem at the ablator-fuel interface [11]. These predicted differences are taken into account when applying a laser pulse tuned in a keyhole target to a layered DT implosion, but to date they have never been experimentally validated. This Letter reports the first experimental validation of the assumptions underlying this surrogate technique as well as presenting the first measurements and analysis of shock mergers in the central DT gas region.

To quantify differences in shock strengths between liquid D2 tuning targets and layered DT ice ignition targets, the keyhole target was modified to allow for the growth of DT ice layers. As the inset of Fig. 1(b) shows, the Au cone presents a severe perturbation to the capsule interior, precluding the growth of a uniform spherical ice layer. Simulations of the cryogenic thermal environment, however, show that with the addition of an external heater (resistive wire wrapped around the Au cone, just outside of the hohlraum), the isotherms in the DT at the cone tip, where the VISAR measurements are made, can be engineered to be locally spherical. The heater power required to grow reasonably uniform ice layers was ~10 mW, a value which is comparable to the heat input used to control the sphericity of ice layers in ignition targets [12]; the heater input should therefore not perturb the hohlraum thermal environment. The mean layer thickness was controlled to an accuracy of <1 μm by the initial gas volume that was injected into the target.

Figure 2(a) shows an x-ray radiograph taken through the laser entrance holes of a "thick" DT ice layer grown on NIF (shot N121101). The tip of the Au cone and the inner surface of the Si-doped CH ablator are clearly seen. The gap between these two surfaces was 400 μm. The interface between the DT ice and the equilibrium DT vapor is visualized by x-ray refraction. The nominal thickness goal of this layer was 300 μm. This value was chosen because the entire shock velocity history such as that shown in Fig. 1 is measured within 200 μm of the ablator inner surface. A DT layer of thickness 300 μm is therefore effectively infinitely thick and is used to provide a direct comparison of shock velocity histories with the continuous D2-filled tuning targets without any complication due to decompression of the ice layer.

In ignition capsules, the best quality DT ice layers are grown from a single seed crystal [12]. The crystal structure (single vs polycrystalline) and orientation in these keyhole ice layers has not yet been characterized, but the surfaces are observed to be very smooth with a small number (typically ≤ 3) of grain boundary "grooves." Future experiments will quantify the crystal structure allowing for the possibility of anisotropic shock speed measurements.

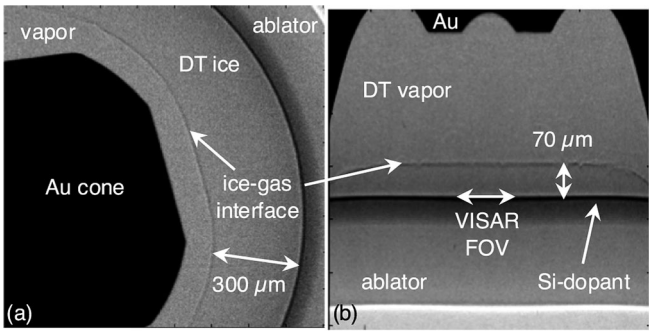

FIG. 2. (a) X-ray radiograph of the capsule interior (shot N121101) showing the tip of the Au diagnostic cone, the Si-doped CH ablator, and the contour of a 300 μm thick DT ice layer. (b) Unwrapped view of a 70 μm thick DT ice layer (shot N121108) showing ice thickness variation relative to the ablator inner surface.

To study the effect of shock release from the layer and ice interfacial decompression into the central DT gas, layers of thickness corresponding to those used in ignition targets (nominal value 70 μm [13]) were grown as well. Figure 2(b) shows an example of such a layer (shot N121108), where the thickness uniformity of the layer is shown by un-wrapping the image relative to the inner surface of the ablator. Figure 2(b) shows nearly the full lateral extent of the layer from the center of the Au cone tip to the azimuthal location where the capsule contacts the cone. In this view, the flat portion of the Au cone tip appears as the curved region in the center. The lateral extent of the VISAR measurements at the ablator inner surface is ~350 μm. The uniformity of the layer thickness over this field of view was better than 1 μm.

Figure 3 shows VISAR streaked interferometer images for three shots: (a) N121112, a standard liquid D2-filled keyhole target, (b) N121101, a thick (300 μm) DT ice layer, and (c) N121108, a thin (70 μm) DT ice layer. Time runs from left to right, and lateral (bottom-to-top) motion of the interference fringes is directly proportional to the shock velocity with fringe motion upward indicating an accelerating shock. The relatively darker fringes at the top and bottom of each image are reflections of the VISAR laser from a stationary Au aperture at the tip of the Au cone as seen in Fig. 1(b). Fringe motion between these stationary references is due to reflections from the leading shock front in the fuel (D2 or DT). Discontinuities in the fringe positions indicate the arrival time of shocks. The first of these, labeled "1" and seen near 14 ns, is the time at which the 1st shock breaks out of the CH ablator into the fuel. Subsequent discontinuities indicate the time at which the increasingly stronger 2nd, 3rd, and 4th shocks overtake or merge with preceding shocks.

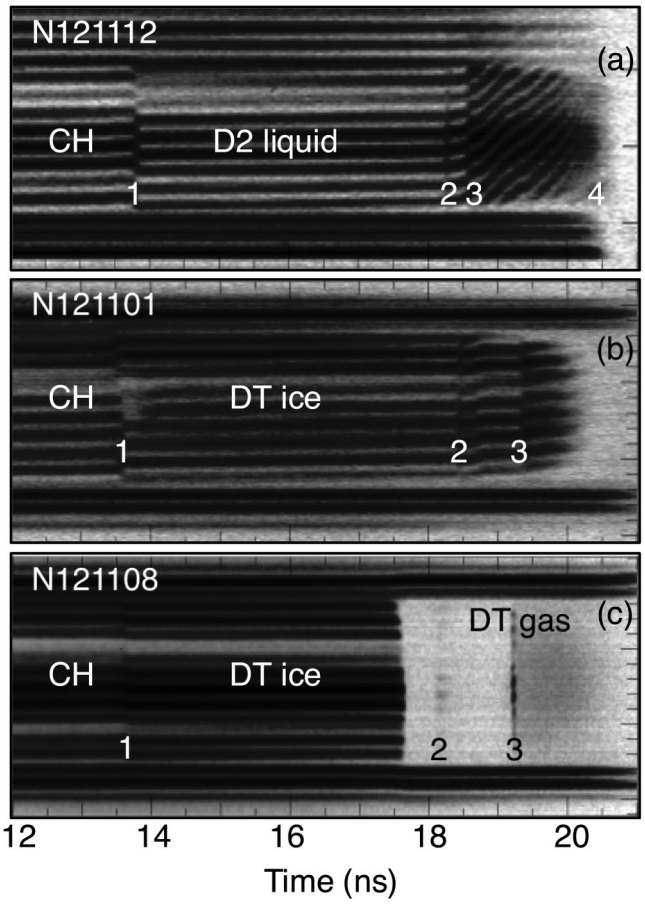

FIG. 3. VISAR streaked interferometer images for (a) shot N121112, a standard liquid D2-filled keyhole tuning target, (b) shot N121101, a 300 μm thick DT ice layer, and (c) shot N121108, a 70 μm thick DT ice layer. Shock mergers 2 and 3 in (c) occur in the expanding DT gas region.

In Figure 3(a), the liquid D2-filled shot, all 4 shocks are seen with the arrival time of shocks 2 and 3 adjusted to be close to that desired for optimal ignition tuning. Figure 3(b) shows very similar results for a thick (300 μm) DT ice layer with the 3rd shock intentionally delayed for better diagnosis of the individual 2nd and 3rd shock velocity levels. Figure 3(c), 70 μm DT ice layer, shows several new features. The VISAR interferometer signal abruptly ceases at $t \approx 17.5 \pm 0.07$ ns, as the 1st shock passes through the DT ice-gas interface (the variation in breakout time is due to a small variation in the layer thickness). The resulting rarefaction reflected from this interface as seen in Fig. 1(a) generates pressure and density gradients in the expanding DT ice. As will be quantified later, the reduced pressure in the expanding ice drops below that required for reflectivity of the VISAR laser ($\lambda = 660$ nm) [6]. As the 2nd and 3rd shocks traverse this decompressing ice region, they briefly recompress it to the pressure level required for VISAR reflection. This is seen in Fig. 3(c) at $t \approx 18.1$ and 19.2 ns as transient increases in the VISAR reflectivity. The weaker signal from 19.2 to 20.5 ns is thermal emission from the stronger 3rd shock; here the VISAR is functioning as a streaked optical pyrometer (SOP) [14,15], recording thermal emission within the band pass of the VISAR. The 4th shock is not seen in either Figs. 3(b) or 3(c) as it was intentionally removed to avoid complications with high-energy Au M-band (2–3 keV) radiation associated with the strong 4th pulse. The 4th pulse timing will be studied in future experiments.

Figure 4 shows a comparison of measured first shock velocities for five shots, which all use the same laser pulse. The velocity histories and shock velocity discontinuities are unambiguously obtained from the VISAR interferometry data using two channels with different velocity sensitivities (see details in [5]). Two liquid-D2 filled shots (N120305, N121112), one performed before and one after the layered DT ice shots, are shown in black. Three layered DT shots (N121101, N121105, N121108) are shown in red, green, and blue, respectively. Small shot-to-shot power variations in the early part of the laser pulse are accounted for by normalizing all shock velocity histories in the CH

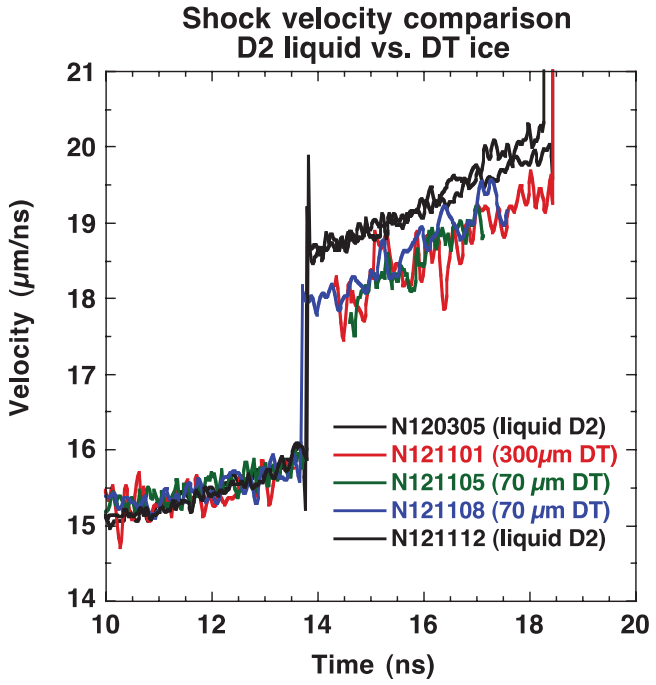

FIG. 4 (color). VISAR-measured first shock velocity histories comparing shock propagation in liquid D2 (N120305, N121112 in black) and DT ice (N121101, N121105, and N11108 in red, green, and blue, respectively).

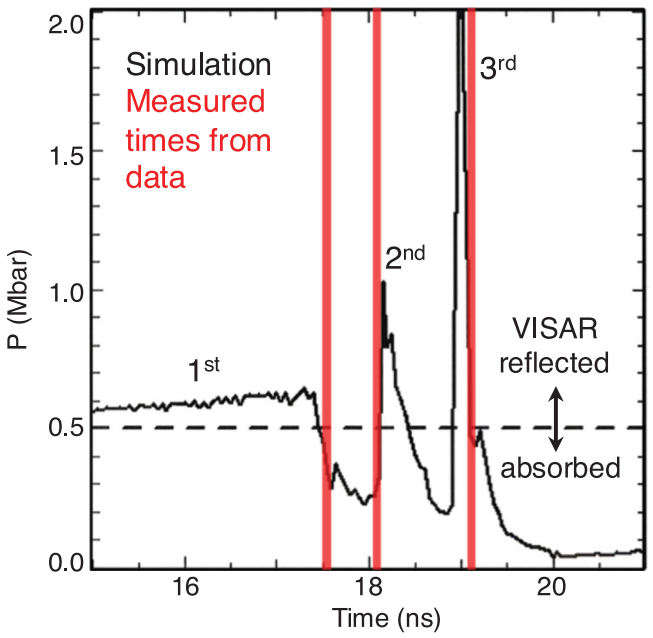

FIG. 5 (color). Plot of simulated pressure vs time at the critical density for absorption of the VISAR laser showing the predicted time history of reflection or absorption of the VISAR probe laser. Red lines indicate the measured time of the 1st shock breakout and 2nd and 3rd shock recompression of the decompressing ice-gas interface for shot N121108. The width of the lines is the measurement error bar of ±50 ps.

ablator. A clear difference is seen with the first shock velocity (averaged from the time of the ablator breakout to the 2nd shock merger) in the more dense DT ice lower by 0.7 μm/ns relative to the D2 liquid. This measurement is in excellent agreement with the predicted difference from numerical simulation (0.9 μm/ns) as shown in the inset velocity list of Fig. 1(b). The difference between measurement and simulation is smaller than the VISAR absolute velocity measurement error bar, which is 0.4 μm/ns. A similar level of agreement is observed for the 2nd and 3rd shock velocities as well, with differences between measurement and simulation of 0.5 and 1.0 μm/ns, respectively. The nominal 2nd and 3rd shock velocities (average of D2 and DT) are 34 and 66 μm/ns, respectively; thus, these differences are both 1.5% of the nominal velocities, well within the ignition requirements of [13].

The surrogacy regarding the presence or absence of an ice-gas interface and the resulting interfacial decompression can be assessed by the data shown in Fig. 3(c). The brief returns of the VISAR reflectivity were attributed to the transient recompression of shocks 2 and 3. This can be compared with predictions from HYDRA simulations by incorporating the VISAR reflectivity measurements of Celliers [6], where it was shown that VISAR reflectivity in liquid D2 has a threshold in both the electron density ($ne > ne_{crit}$) and the pressure ($P > 0.5$ Mbar). A metric for VISAR reflectivity from the simulations is determined by the following procedure. The electron density seen by the VISAR laser as it propagates through the fuel toward the shock front is quantified. When the probe laser reaches the critical density (satisfying the first VISAR reflectivity criterion), the pressure is recorded. Figure 5 plots this simulated pressure history (black) for a 70 μm thick DT ice layer (N121108). The first shock shows a pressure of 0.6–0.7 Mbar as it slowly accelerates in its transit of the ice layer. At $t = 17.6$ ns, the shock breaks out of the ice layer and the simulated pressure at critical density decreases rapidly to a value below the 0.5 Mbar threshold for reflectivity. As the 2nd and 3rd shocks recompress this decompressing ice layer, the simulated pressure briefly jumps back across this threshold, predicting a return of reflectivity of the VISAR probe laser. The red lines show the corresponding measured times from the data of Fig. 3(c) for 1st shock breakout and recompression by the 2nd and 3rd shocks. The width of the lines gives the error bar on the measurement (± 50 ps). The agreement between data and simulation is within 100 ps for all three measurements, again well within ignition requirements [13]. It is important to note that these simulations use an identical drive source (with a 10% correction to the laser power in the trough to give good agreement with the liquid D2 data) and the same equations of state and opacities. This normalization to the D2 data serves to isolate any additional effects due to the change of species, densities, or the added interface of the layered DT experiments. The comparison of

Fig. 5 provides the first data on shock mergers in expanding DT gas and provides a validation of the simulations in this regime of the implosions.

These data give the first experimental measurements confirming the predicted shock propagation in DT ice layers and in the decompressing material following shock transit into the central gas. Together, these data confirm the surrogacy assumptions underlying the tuning technique that is being used to optimize compression in both directly driven and indirectly driven ICF implosions. These initial experiments also demonstrate for the first time a measurement platform that can be used for further assessment of the properties of solid DT (e.g., equations of state) that are critical to the advancement of inertial confinement fusion. Additional experiments are being planned to take advantage of this new capability.

This work was performed under the auspices of the Lawrence Livermore National Security, LLC, (LLNS) under Contract No. DE-AC52-07NA27344.

*robey1@llnl.gov

[1] J. D. Lindl, P. Amendt, R. L. Berger, S. G. Glendinning, S. H. Glenzer, S. W. Haan, R. L. Kauffman, O. L. Landen, and L. J. Suter, Phys. Plasmas **11**, 339 (2004).

[2] M. M. Marinak, G. D. Kerbel, N. A. Gentile, O. Jones, D. Munro, S. Pollaine, T. R. Dittrich, and S. W. Haan, Phys. Plasmas **8**, 2275 (2001).

[3] D. H. Munro, P. M. Celliers, G. W. Collins, D. M. Gold, L. B. Da Silva, S. W. Haan, R. C. Cauble, B. A. Hammel, and W. W. Hsing, Phys. Plasmas **8**, 2245 (2001).

[4] L. M. Barker and R. E. Hollenbach, J. Appl. Phys. **43**, 4669 (1972).

[5] P. M. Celliers, D. K. Bradley, G. W. Collins, D. G. Hicks, T. R. Boehly, and W. J. Armstrong, Rev. Sci. Instrum. **75**, 4916 (2004).

[6] P. M. Celliers, G. Collins, L. Da Silva, D. Gold, R. Cauble, R. Wallace, M. Foord, and B. Hammel, Phys. Rev. Lett. **84**, 5564 (2000).

[7] T. R. Boehly, Phys. Plasmas **16**, 056302 (2009).

[8] T. R. Boehly, V. N. Goncharov, W. Seka, M. A. Barrios, P. M. Celliers, D. G. Hicks, G. W. Collins, S. X. Hu, J. A. Marozas, and D. D. Meyerhofer, Phys. Rev. Lett. **106**, 195005 (2011).

[9] H. F. Robey *et al.*, Phys. Plasmas **19**, 042706 (2012).

[10] H. F. Robey *et al.*, Phys. Rev. Lett. **108**, 215004 (2012).

[11] E. F. Toro, *Riemann Solvers and Numerical Methods for Fluid Dynamics* (Springer Verlag, Berlin, 1999).

[12] B. J. Kozioziemski, E. R. Mapoles, J. D. Sater, A. A. Chernov, J. D. Moody, J. B. Lugten, and M. A. Johnson, Fusion Sci. Technol. **59**, 14 (2011).

[13] S. W. Haan *et al.*, Phys. Plasmas **18**, 051001 (2011).

[14] R. J. Trainor, J. W. Shaner, J. M. Auerbach, and N. C. Holmes, Phys. Rev. Lett. **42**, 1154 (1979).

[15] J. E. Miller, T. R. Boehly, A. Melchior, D. D. Meyerhofer, P. M. Celliers, J. H. Eggert, D. G. Hicks, C. M. Sorce, J. A. Oertel, and P. M. Emmel, Rev. Sci. Instrum. **78**, 034903 (2007).